Journal of Computational Physics 242 (2013) 351–366

Contents lists available at SciVerse ScienceDirect

Journal of Computational Physics

journal homepage: www.elsevier.com/locate/jcp

A direct discontinuous Galerkin method for the generalized Korteweg–de Vries equation: Energy conservation and boundary effect

Nianyu Yi [a], Yunqing Huang [a], Hailiang Liu [b,*]

[a] Hunan Key Laboratory for Computation and Simulation in Science and Engineering, School of Mathematics and Computational Science, Xiangtan University, Xiangtan 411105, PR China

[b] Iowa State University, Mathematics Department, Ames, IA 50011, United States

ARTICLE INFO

Article history:
Received 9 August 2012
Received in revised form 12 December 2012
Accepted 24 January 2013
Available online 14 February 2013

Keywords:
Direct discontinuous Galerkin method
Korteweg–de Vries
Conservation
Stability

ABSTRACT

A direct discontinuous Galerkin method for solving the generalized Korteweg–de Vries (KdV) equation with both periodic data and non-homogeneous boundary data is developed. A class of numerical fluxes is identified so that the method preserves both momentum and energy for the initial value problem. The method with such a property is numerically shown robust with less error in both phase and amplitude after long time simulation. Numerical examples are given to confirm the theoretical result and the capacity of this method for capturing soliton wave phenomena and various boundary wave patterns.

Published by Elsevier Inc.

1. Introduction

This paper is concerned with the numerical approximation of the one dimensional generalized Korteweg–de Vries (KdV) [21] equation

$$u_t + f(u)_x + \epsilon u_{xxx} = 0, \tag{1.1}$$

where ϵ is a given constant, and f is a smooth function. This is a nonlinear, dispersive partial differential equation for u of two real variables, space x and time t. The original form of the KdV equation corresponds to $\epsilon = 1$ and $f = 3u^2$. The KdV equation has several connections to physical problems. In addition to being the governing equation of the string in the Fermi–Pasta–Ulam problem in the continuum limit, it approximately describes the evolution of long, one-dimensional waves in many physical settings, including shallow-water waves with weakly non-linear restoring forces, long internal waves in a density-stratified ocean, ion-acoustic waves in a plasma, acoustic waves on a crystal lattice, and more.

Dispersion and non-linearity can interact to produce permanent and localized wave forms; It can be shown that any sufficiently fast decaying smooth solution will eventually split into a finite superposition of solitons traveling to the right plus a decaying dispersive part traveling to the left. This was first observed numerically by Zabusky & Kruskal (1965) [42], long after John Scott Russell's experimental observation of solitons in 1834. One appealing feature of the KdV equation is that it has infinitely many integrals of motion [30], which do not change with time. This is also accounted by the fact that the KdV equation can be reformulated into the Lax system, called Lax pairs (1968) [22]. The first two integrals of motion for the KdV equation and the generalized one are

* Corresponding author.
E-mail addresses: yinianyu365109@126.com (N. Yi), huangyq@xtu.edu.cn (Y. Huang), hliu@iastate.edu (H. Liu).

0021-9991/$ - see front matter Published by Elsevier Inc.
http://dx.doi.org/10.1016/j.jcp.2013.01.031

$$\text{the momentum} = \int u dx, \quad \text{the energy} = \int u^2 dx. \tag{1.2}$$

The purpose of this paper is to design a method that preserves these two conserved integrals.

The concept of 'energy' has far-reaching importance throughout the physical sciences. The conservation law structure of many PDEs is considered fundamental to their derivation, their behavior, and their discretization. For conservative PDEs, numerical methods preserving their invariants are often advantageous: besides the high accuracy of numerical solutions, a conservative scheme can preserve good stability properties after long-time numerical integration. There are many numerical works in the literature to solve the KdV equation, ranging from finite difference methods [13–15,23,35,42], finite element methods [1,31,34], spectral methods [12,16,20,27,28,32], operator splitting methods [17,18], and discontinuous Galerkin methods [5,24,36,37,40]. However, the majority of the developed methods is designed to preserve the momentum, not the energy; as a consequence, the resulting scheme can suffer certain accuracy loss, particularly phase/amplitude errors are often observed in the long time simulation of soliton waves.

The goal of this paper is to develop a discontinuous Galerkin (DG) method to preserve both momentum and energy at the discrete setting. The earlier effort of inheriting some invariants as characteristic properties followed mainly the symplectic method for Hamiltonian ODEs; for instance, Furihata [13] designed a finite difference scheme to preserve momentum and $\int G dx$ with $G = \frac{1}{6}u^3 - \frac{1}{2}(u_x)^2$ based on the reformulation of the form $\partial_t u = \partial_x \partial_u G$. See also the discussion comparing different constructions of energy-preserving integrators in [11]. Cui and Mao [6] developed a finite difference method preserving both momentum and energy, by discretizing a coupled system for (u, u^2). A direct finite difference method preserving (1.2) was further introduced in the PhD thesis of Xie [35] under the supervision of H.-L. Liu. Recently a significant step has been taken by Bona et al. [2] to develop a discontinuous Galerkin method for the KdV equation to preserve the first two integrals of motion. Furthermore, they are able to prove that the order of accuracy of the semi-discrete approximation is suboptimal, provided the degree of the polynomial elements is even and that the number of computational cells is odd. While, error estimates in other cases remain unsettled.

In this work we design a direct discontinuous Galerkin (DDG) method, in contrast to the local discontinuous Galerkin (LDG) methods previously developed in [24,36,37,40] for KdV type equations. The term DDG, following from [25,26] by Liu and Yan primarily for diffusion problems, refers to that the discretization is a direct DG projection of the PDE weak formulation, necessarily refined by interface corrections due to the use of discontinuous elements. One main advantage of such methods is the use of special numerical fluxes such that the numerical scheme is not only highly accurate but also conserve some desired quantities, without writing the equation into a first order system. There are several novel aspects in this work when put in comparison with [2]: the DDG formulation presented in this work is local, and a class of numerical fluxes is identified for the scheme to preserve two integrals (1.2). The global version of our scheme for the initial value problem (IVP) when a particular numerical flux is taken, plus further integration by parts on the u_{xxx} term, can be recast into the form as introduced in [2] for $f = u^{p+1}$. We also extend the energy preserving DDG scheme to the case with non-homogeneous boundary conditions and prove the stability of the resulting schemes for the initial boundary value problem (IBVP), therefore also improving upon the earlier work [24].

The discontinuous Galerkin (DG) method we discuss in this paper is a class of finite element methods using completely discontinuous piecewise-polynomial spaces for the numerical solution and the test functions. It was first designed and has been successful for solving first order PDEs such as hyperbolic conservation laws [33,8,7,9,10], and have been extended to various PDEs by many authors, e.g., [4,19,38,39,41]. These discontinuous Galerkin methods have several attractive properties. For instance, it can be easily designed for any order of accuracy, which can be locally determined in each cell, thus allowing for efficient p adaptivity. The methods are extremely local in data communications: the evolution of the solution in each cell needs to communicate only with the immediate neighbors, regardless of the order of accuracy, among other nice properties.

The organization of the paper is as follows. In Section 2, we present a DDG method for the IVP, further analyze and validate the conservative properties of the method. In Section 3, we present the DDG method for the IBVP, by considering general non-homogeneous boundary conditions, and prove the nonlinear L^2 stability of the method. All numerical examples are presented in Section 4.

Our numerical results for the IVP show that the convergence rate for even-order elements is optimal, whilst, for odd-order elements, the convergence rate is suboptimal. For the quadratic element, the convergence rate is fourth order, which illustrates certain superconvergence. The numerical results for the IBVP show that the convergence rate is optimal for both even-order elements and odd-order elements. The capacity of our method in capturing the correct boundary wave patterns is also verified, and results are consistent with the wave patterns studied in [29] and numerically tested in [24] by the LDG method.

2. The initial value problem (IVP)

In this section, we consider the initial value problem of the generalized KdV equation,

$$\begin{cases} u_t + (f(u))_x + \epsilon u_{xxx} = 0, & x \in (L, R), t > 0, \\ u(x, 0) = u_0(x), & x \in (L, R), \end{cases} \tag{2.1}$$

with periodic boundary conditions. We denote the computational cell by $I_j = (x_{j-1/2}, x_{j+1/2})$ for $j = 1, \ldots, N$. The center of the cell is $x_j = (x_{j-1/2} + x_{j+1/2})/2$, and $h_j = x_{j+1/2} - x_{j-1/2}$. We denote by $v^+_{j+1/2}$ the value of v at $x_{j+1/2}$ evaluated from the right element I_{j+1}, and $v^-_{j+1/2}$ the value of v at $x_{j+1/2}$ evaluated from the left element I_j. $[v] = v^+ - v^-$ denotes the jump of v at cell interfaces, and $\{v\} = \frac{1}{2}(v^+ + v^-)$ denotes the average of the left and right boundary values. We then define the piecewise polynomial space V_h as the space of polynomials of degree k in each cell I_j, i.e.,

$$V_h = \{v : v \in P^k(I_j) \text{ for } x \in I_j, j = 1, \ldots, N\}.$$

2.1. The DDG scheme

In order to design a discontinuous Galerkin method for the generalized KdV Eq. (2.1), which can preserve both momentum and energy at the semi-discrete level, we adopt the DDG methodology by a direct spatial DG discretization of the weak formulation of (2.1) on each cell, balanced with proper interface corrections. More precisely, the semi-discrete approximation for the initial value problem of (2.1) with periodic boundary conditions reads: to find $u_h \in V_h$, such that

$$\int_{I_j} u_{ht} v dx - \int_{I_j} f(u_h) v_x dx - \epsilon \int_{I_j} u_{hxx} v_x dx + \widehat{f}(u_h) v \Big|_{j-\frac{1}{2}}^{j+\frac{1}{2}} + \epsilon \widehat{u_{hxx}} v \Big|_{j-\frac{1}{2}}^{j+\frac{1}{2}} + \epsilon (u_{hx} - \widehat{u_{hx}}) v_x \Big|_{j-\frac{1}{2}}^{j+\frac{1}{2}} + \epsilon (\widehat{u_h} - u_h) v_{xx} \Big|_{j-\frac{1}{2}}^{j+\frac{1}{2}} = 0 \tag{2.2}$$

holds for any $v \in V_h$, where the values of functions v, v_x, v_{xx} at interfaces $x_{j\pm1/2}$ are evaluated from within the cell I_j, and the "hat" terms are numerical fluxes to be selected so that numerical solutions of (2.2) satisfy the following conservative properties,

$$\frac{d}{dt} \int_L^R u_h dx = 0, \quad \frac{d}{dt} \int_L^R u_h^2 dx = 0, \tag{2.3}$$

as exact solutions of the PDE do. To be more specific, we assume the numerical fluxes $\widehat{u_{hxx}}, \widehat{u_{hx}}, \widehat{u_h}$ are in weighted averaging form

$$\begin{aligned} \widehat{u_{hxx}} &= \theta u^+_{hxx} + (1-\theta) u^-_{hxx}, \\ \widehat{u_{hx}} &= \beta u^+_{hx} + (1-\beta) u^-_{hx}, \\ \widehat{u_h} &= \gamma u^+_h + (1-\gamma) u^-_h, \end{aligned} \tag{2.4}$$

with weight parameters θ, β and γ to be determined.

Summing Eq. (2.2) over all I_j, subject to some algebraic manipulation, we obtain

$$\begin{aligned} &\sum_{j=1}^N \int_{I_j} u_{ht} v dx - \sum_{j=1}^N \int_{I_j} f(u_h) v_x dx - \epsilon \sum_{j=1}^N \int_{I_j} u_{hxx} v_x dx - \sum_{j=1}^N (\widehat{f}(u_h)[v])_{j-\frac{1}{2}} - \epsilon \sum_{j=1}^N (\widehat{u_{hxx}}[v])_{j-\frac{1}{2}} \\ &\quad - \epsilon \sum_{j=1}^N \left([u_{hx} v_x] - \widehat{u_{hx}}[v_x]\right)_{j-\frac{1}{2}} - \epsilon \sum_{j=1}^N \left(\widehat{u_h}[v_{xx}] - [u_h v_{xx}]\right)_{j-\frac{1}{2}} = 0. \end{aligned} \tag{2.5}$$

By choosing $v = 1$ in (2.5), one can verify that the momentum is conserved. Taking the test function $v = u_h$ in (2.5), we have

$$\sum_{j=1}^N \int_{I_j} u_{ht} u_h dx + \sum_{j=1}^N \left(\int_{u^-_h}^{u^+_h} f(u) du - \widehat{f}(u_h)[u_h] \right)_{j-\frac{1}{2}} - \epsilon \sum_{j=1}^N \left(\frac{1}{2}[u^2_{hx}] - \widehat{u_{hx}}[u_{hx}] + \widehat{u_{hxx}}[u_h] + \widehat{u_h}[u_{hxx}] - [u_h u_{hxx}] \right)_{j-\frac{1}{2}} = 0. \tag{2.6}$$

To ensure the energy conservation, it suffice to require the following

$$\int_{u^-_h}^{u^+_h} f(u) du - \widehat{f}(u_h)[u_h] = 0, \tag{2.7}$$

$$\frac{1}{2}[u^2_{hx}] - \widehat{u_{hx}}[u_{hx}] + \widehat{u_{hxx}}[u_h] + \widehat{u_h}[u_{hxx}] - [u_h u_{hxx}] = 0, \tag{2.8}$$

at all cell interfaces. Substituting (2.4) into (2.8), we find

$$\begin{aligned} &\beta u^+_{hx} + (1-\beta) u^-_{hx} - \{u_{hx}\} = 0, \\ &(\theta + \gamma - 1)(u^+_h u^+_{hxx} + u^-_h u^-_{hxx} - u^+_h u^-_{hxx} - u^-_h u^+_{hxx}) = 0, \end{aligned} \tag{2.9}$$

then the weights $\theta, \beta, \gamma \in [0, 1]$ necessarily satisfy

$$\beta = \frac{1}{2}, \quad \theta + \gamma = 1. \tag{2.10}$$

This leads to the following numerical fluxes

$$\widehat{f}(u_h) = \fint_{u_h^-}^{u_h^+} f(u)du := \frac{\int_{u_h^-}^{u_h^+} f(u)du}{u_h^+ - u_h^-} \tag{2.11}$$

and

$$\begin{aligned} \widehat{u_{hxx}} &= u_{hxx}^{\theta} := \theta u_{hxx}^+ + (1-\theta)u_{hxx}^-, \\ \widehat{u_{hx}} &= \{u_{hx}\} := \frac{u_{hx}^+ + u_{hx}^-}{2}, \\ \widehat{u_h} &= u_h^{1-\theta} := (1-\theta)u_h^+ + \theta u_h^-, \end{aligned} \tag{2.12}$$

with $\theta \in [0,1]$. With these choices, this θ-class of schemes (2.2) is well defined, and satisfies the desired conservative properties, as summarized in the following.

Theorem 2.1. *The numerical scheme (2.2) with numerical fluxes (2.11) and (2.12) satisfies the conservative properties,*

$$\frac{d}{dt}\int_L^R u_h dx = 0, \tag{2.13}$$

$$\frac{d}{dt}\int_L^R u_h^2 dx = 0. \tag{2.14}$$

Then the DDG scheme is L^2 stable,

$$\|u_h(t)\| = \|u_h(0)\| \tag{2.15}$$

for all $t \geqslant 0$.

Two remarks are in order.

Remark 2.1. Extensive numerical tests indicate that the choice of parameter θ has certain effects on the accuracy in terms of the error of the numerical solution, instead of the orders of accuracy.

Remark 2.2. The global form of the DG formulation may be obtained by summing over all j's,

$$(u_{ht}, v) + (\mathcal{N}(u_h), v) + \epsilon(\mathcal{D}_\theta(u_h), v) = 0, \quad \forall v \in V_h, \tag{2.16}$$

where

$$(\mathcal{N}(u_h), v) = -\sum_{j=1}^N (f(u_h), v_x)_{I_j} - \sum_{j=1}^N \widehat{f}(u_h)_{j-\frac{1}{2}}[v]_{j-\frac{1}{2}}, \tag{2.17}$$

$$\begin{aligned} (\mathcal{D}_\theta(u_h), v) = &-\sum_{j=1}^N (u_{hxx}, v_x)_{I_j} - \sum_{j=1}^N [u_{hx}]_{j-\frac{1}{2}}\{v_x\}_{j-\frac{1}{2}} \\ &- \sum_{j=1}^N \Big(\big(\theta u_{hxx}^+ + (1-\theta)u_{hxx}^-\big)_{j-\frac{1}{2}}[v]_{j-\frac{1}{2}} - [u_h]_{j-\frac{1}{2}}\big(\theta v_{xx}^+ + (1-\theta)v_{xx}^-\big)_{j-\frac{1}{2}}\Big). \end{aligned} \tag{2.18}$$

If we take $\theta = 1$ and rewrite $\sum_{j=1}^N (u_{hxx}, v_x)_{I_j} = -\sum_{j=1}^N (u_{hx}, v_{xx})_{I_j} - \sum_{j=1}^N [u_{hx} v_x]_{j-\frac{1}{2}}$, then we find the DG scheme introduced in [2] for the KdV Eq. (2.1) with $f(u) = u^{p+1}$. Note that our scheme is derived by integration by parts once for the dispersive term u_{xxx}, while the scheme presented in [2] uses integration by parts twice, and the scheme developed by Cheng and Shu [5] applies integration by parts three times.

2.2. Time discretization

To ensure the fully-discrete scheme still preserves the conservation properties of the semi-discrete approximations, the time discretization should be chosen carefully. We consider the Crank-Nicolson time discretization.

Let $\{t^n\}, n = 0, 1, \ldots, M$ be a uniform partition of the time interval $[0, T]$. Set $\Delta t = t^{n+1} - t^n$ as the time step. Define $u_h^{n+1/2} = \frac{u_h^{n+1} + u_h^n}{2}$. The fully-discrete DDG method for the KdV equation is to find $u_h^n \in V_h$ such that

$$\int_{I_j} \frac{u_h^{n+1}-u_h^n}{\Delta t} v dx - \int_{I_j} f(u_h^{n+1/2}) v_x dx - \epsilon \int_{I_j} u_{hxx}^{n+1/2} v_x dx + \widehat{f}(u_h^{n+1/2}) v \Big|_{j-\frac{1}{2}}^{j+\frac{1}{2}} + \epsilon \widehat{u_{hxx}^{n+1/2}} v \Big|_{j-\frac{1}{2}}^{j+\frac{1}{2}}$$
$$+ \epsilon \left(u_{hx}^{n+1/2} - \widehat{u_{hx}^{n+1/2}} \right) v_x \Big|_{j-\frac{1}{2}}^{j+\frac{1}{2}} + \epsilon \left(\widehat{u_h^{n+1/2}} s - u_h^{n+1/2} \right) v_{xx} \Big|_{j-\frac{1}{2}}^{j+\frac{1}{2}} = 0, \tag{2.19}$$

with $u_h^0 = Pu_0$, the piecewise L^2 projection of $u_0(x)$.

With such a time discretization, the fully-discrete scheme preserves the desired conservation properties.

Theorem 2.2. *The fully-discrete approximation u_h^n satisfies*

$$\int_L^R u_h^n dx = \int_L^R u_h^0 dx, \tag{2.20}$$
$$\|u_h^n\| = \|u_h^0\| \tag{2.21}$$

for all $0 \leqslant n \leqslant M$.

Proof. Take the test function $v = 1$ in (2.19) and sum over all j to obtain

$$\sum_j \int_{I_j} \frac{u_h^{n+1}-u_h^n}{\Delta t} dx = \int_L^R \frac{u_h^{n+1}-u_h^n}{\Delta t} dx = 0,$$

which leads to (2.20).

Taking $v = u_h^{n+1/2}$ in (2.19), summing over j and after similar algebraic manipulation to that leading to Theorem 2.1, we obtain

$$\sum_j \int_{I_j} \frac{u_h^{n+1}-u_h^n}{\Delta t} u_h^{n+1/2} dx = \sum_j \int_{I_j} \frac{(u_h^{n+1})^2 - (u_h^n)^2}{2\Delta t} dx = 0.$$

Hence

$$\int_L^R (u_h^{n+1})^2 dx = \int_L^R (u_h^n)^2 dx,$$

leading to (2.21), as desired. □

3. The initial boundary value problem (IBVP)

For the IBVP with general boundary conditions, we restrict to the case of ϵ being positive. In this section, we consider the KdV equation posed on a finite domain $x \in [L, R]$, subject to both initial and boundary conditions,

$$\begin{cases} u_t + f(u)_x + \epsilon u_{xxx} = 0, & x \in [L,R], \\ u(x,0) = u_0(x), & x \in [L,R], \\ u(L,t) = a_1(t), u(R,t) = a_2(t), & t > 0, \\ u_x(R,t) = b(t), & t > 0. \end{cases} \tag{3.1}$$

Remark 3.1. If ϵ is negative, the boundary conditions should be given differently for the well-posedness, one option given in [24] is

$$\begin{cases} u(L,t) = a_1(t), u(R,t) = a_2(t), & t > 0, \\ u_x(L,t) = b(t), & t > 0. \end{cases}$$

3.1. The DDG scheme

The DDG approximation for KdV Eq. (3.1) is to find $u_h \in V_h$ such that

$$\int_{I_j} u_{ht} v dx - \int_{I_j} f(u_h) v_x dx - \epsilon \int_{I_j} u_{hxx} v_x dx + \widehat{f}(u_h) v \Big|_{j-\frac{1}{2}}^{j+\frac{1}{2}} + \epsilon \widehat{u_{hxx}} v \Big|_{j-\frac{1}{2}}^{j+\frac{1}{2}} + \epsilon (u_{hx} - \widehat{u_{hx}}) v_x \Big|_{j-\frac{1}{2}}^{j+\frac{1}{2}} + \epsilon (\widehat{u_h} - u_h) v_{xx} \Big|_{j-\frac{1}{2}}^{j+\frac{1}{2}} = 0, \ \forall v \in V_h,$$

$$\int_L^R (u_h(0) - u_0) v dx = 0, \ \forall v \in V_h. \tag{3.2}$$

At the inner cell interface $x_{j+\frac{1}{2}}, j = 1, 2, \ldots, N-1$ the numerical fluxes are set by

$$\widehat{f}(u_h) = \frac{\int_{u_h^-}^{u_h^+} f(u) du}{u_h^+ - u_h^-} \tag{3.3}$$

and

$$\begin{aligned} \widehat{u_{hxx}} &= u_{hxx}^{\theta} := \theta u_{hxx}^+ + (1-\theta) u_{hxx}^-, \\ \widehat{u_{hx}} &= \{u_{hx}\} := \frac{u_{hx}^+ + u_{hx}^-}{2}, \\ \widehat{u_h} &= u_h^{1-\theta} := (1-\theta) u_h^+ + \theta u_h^-, \end{aligned} \tag{3.4}$$

with $\theta \in [0,1]$. Following [24], we build boundary conditions into the scheme in such a way that the boundary data are used when available, otherwise we use the value of the numerical solution in corresponding end cells. Thus, for the left boundary fluxes, we choose

$$\widehat{f}(u_h)|_{\frac{1}{2}} = \frac{\int_{a_1(t)}^{(u_h)_{1/2}^+} f(u) du}{(u_h)_{1/2}^+ - a_1(t)} \tag{3.5}$$

and

$$(\widehat{u_{hxx}})_{\frac{1}{2}} = (u_{hxx})_{\frac{1}{2}}^+, \quad (\widehat{u_{hx}})_{\frac{1}{2}} = (u_{hx})_{\frac{1}{2}}^+, \quad (\widehat{u_h})_{\frac{1}{2}} = a_1(t). \tag{3.6}$$

For the right boundary fluxes, we set

$$\widehat{f}(u_h)|_{N+\frac{1}{2}} = \frac{\int_{(u_h)_{N+1/2}^-}^{a_2(t)} f(u) du}{a_2(t) - (u_h)_{N+1/2}^-} \tag{3.7}$$

and

$$(\widehat{u_{hxx}})_{N+\frac{1}{2}} = (u_{hxx})_{N+\frac{1}{2}}^-, \quad (\widehat{u_{hx}})_{\frac{1}{2}} = b(t), \quad (\widehat{u_h})_{N+\frac{1}{2}} = a_2(t). \tag{3.8}$$

3.2. Stability analysis

In this subsection, we derive the L^2 stability estimation for $f(u) = \frac{u^2}{2}$, we use a simple transformation

$$w = u + A(t)x + B(t), \quad A(t) = \frac{a_1 - a_2}{R - L}, \quad B(t) = \frac{L a_2 - R a_1}{R - L}, \tag{3.9}$$

which converts problem (3.1) into the following auxiliary problem:

$$\begin{cases} w_t + f(w,x,t)_x + \epsilon w_{xxx} = r(x,t), & x \in [L,R], \\ w(x,0) = w_0(x), & x \in [L,R], \\ w(L,t) = 0, \ w(R,t) = 0, & t > 0, \\ w_x(R,t) = g(t), & t > 0, \end{cases} \tag{3.10}$$

where $f(w,x,t) := f(u) = \frac{(w - A(t)x - B(t))^2}{2}$ and

$$g(t) = b(t) + \frac{a_1 - a_2}{R - L}, \quad r(x,t) = \frac{\dot{a}_1 - \dot{a}_2}{R - L} x + \frac{L\dot{a}_2 - R\dot{a}_1}{R - L}.$$

If w solves the above IBVP, then

$$\begin{aligned}\frac{1}{2}\frac{d}{dt}\|w(\cdot,t)\|^2 &= (w,w_t) = (w,r(x,t)-f(w,x,t)_x-\epsilon w_{xxx})\\ &= \int_L^R wrdx - \int_L^R (w-A(t)x-B(t))(w_x-A(t))wdx - \epsilon\int_L^R\left(ww_{xx}-\frac{w_x^2}{2}\right)_x dx\\ &= \int_L^R wrdx + \frac{1}{2}\int_L^R A(t)w(w-2(A(t)x+B(t)))dx + \frac{\epsilon}{2}g^2(t) - \frac{\epsilon}{2}w_x^2(L,t).\end{aligned}$$

Using the boundary data and the Schwartz inequality, we have

$$\frac{d}{dt}\|w(\cdot,t)\|^2 \leqslant (1+2|A(t)|)\|w(\cdot,t)\|^2 + (\epsilon g^2(t) + |A(t)|\|A(t)x+B(t)\|^2 + \|r(\cdot,t)\|^2).$$

By the Gronwall inequality, we derive an energy estimate for the auxiliary problem (3.10):

$$\|w(\cdot,t)\|^2 \leqslant e^{\int_0^t(1+2|A(\tau)|)d\tau}\left\{\|w(0)\|^2 + \int_0^t\left(\epsilon g^2(\tau) + |A(\tau)|\|A(\tau)x+B(\tau)\|^2 + \|r(x,\tau)\|^2\right)d\tau\right\} \tag{3.11}$$

for any $0 \leqslant t \leqslant T$.

Using the transformation (3.9), we obtain the estimate for the original problem (3.1) with $f(u)=\frac{u^2}{2}$ as the following:

$$\|u(\cdot,t)\| \leqslant K(a_1(t),a_2(t),b(t),\|u(0)\|), \quad \forall t\in[0,T].$$

The DDG method for problem (3.10) is

$$\begin{aligned}&\int_{I_j} w_{ht}vdx - \int_{I_j} f(w_h,x,t)v_x dx - \epsilon\int_{I_j} w_{hxx}v_x dx + \widehat{f}(w_h,x,t)v\Big|_{j-\frac12}^{j+\frac12} + \epsilon\widehat{w_{hxx}}v\Big|_{j-\frac12}^{j+\frac12} + \epsilon(w_{hx}-\widehat{w_{hx}})v_x\Big|_{j-\frac12}^{j+\frac12} + \epsilon(\widehat{w_h}-w_h)v_{xx}\Big|_{j-\frac12}^{j+\frac12}\\ &\quad = (r(x,t),v),\ \forall v\in V_h.\end{aligned} \tag{3.12}$$

The numerical fluxes are derived from Eqs. (3.3)–(3.8),

$$\widehat{f}(w_h,x,t)|_{j+\frac12} = \begin{cases}\left.\dfrac{\int_{w_h^-}^{w_h^+} f(w,x,t)dw}{w_h^+-w_h^-}\right|_{j+\frac12}, & j=1,\dots,N-1,\\ \dfrac{\int_0^{(w_h)_{1/2}^+} f(w,x,t)dw}{(w_h)_{1/2}^+-0}, & j=0,\\ \dfrac{\int_{(w_h)_{N+1/2}^-}^0 f(w,x,t)dw}{0-(w_h)_{N+1/2}^-}, & j=N\end{cases} \tag{3.13}$$

and

$$\left((\widehat{w_{hxx}})_{j+\frac12},(\widehat{w_{hx}})_{j+\frac12},(\widehat{w_h})_{j+\frac12}\right) = \begin{cases}\left((w_{hxx})_{j+\frac12}^{\theta},\{(w_{hx})_{j+\frac12}\},(w_h)_{j+\frac12}^{1-\theta}\right), & j=1,\dots,N-1,\\ ((w_{hxx})_{\frac12}^+,(w_{hx})_{\frac12}^+,0), & j=0,\\ ((w_{hxx})_{N+\frac12}^-,g(t),0), & j=N.\end{cases} \tag{3.14}$$

We now show that the obtained DDG numerical solution is stable. We first prove that the DDG method for the auxiliary problem is L^2 stable in the sense to satisfy (3.11), we then establish the stability of the DDG method for the original IBVP.

Proposition 3.1. *The L^2 norm of the DDG approximation w_h of (3.10) is bounded by initial and boundary conditions as*

$$\|w_h(\cdot,t)\|^2 \leqslant e^{\int_0^t(1+2|A(\tau)|)d\tau}\left\{\|w_h(0)\|^2 + \int_0^t\left(\epsilon g^2(\tau) + |A(\tau)|\|A(\tau)x+B(\tau)\|^2 + \|r(x,\tau)\|^2\right)d\tau\right\}$$

for $0<t\leqslant T$.

Proof. Let $F(w,x,t)=\int_0^w f(s,x,t)ds$, we have

$$f(w,x,t)w_x(x,t) = \frac{\partial F(w,x,t)}{\partial w}w_x(x,t) = \frac{dF(w,x,t)}{dx} + \int_0^w (s-A(t)x-B(t))A(t)ds. \tag{3.15}$$

Since (3.12) holds for any test function in V_h. Let $v=w_h$ in (3.12),

$$\int_{I_j} w_{ht} w_h dx - \int_{I_j} f(w_h, x, t) w_{hx} dx - \epsilon \int_{I_j} w_{hxx} w_{hx} dx + \widehat{f}(w_h, x, t) w_h \Big|_{j-\frac{1}{2}}^{j+\frac{1}{2}} + \epsilon \widehat{w_{hxx}} w_h \Big|_{j-\frac{1}{2}}^{j+\frac{1}{2}} + \epsilon (w_{hx} - \widehat{w_{hx}}) w_{hx} \Big|_{j-\frac{1}{2}}^{j+\frac{1}{2}}$$
$$+ \epsilon (\widehat{w_h} - w_h) w_{hxx} \Big|_{j-\frac{1}{2}}^{j+\frac{1}{2}} = \int_{I_j} r w_h dx. \tag{3.16}$$

Applying (3.15), second term in Eq. (3.16) becomes

$$-\int_{I_j} \frac{dF(w_h, x, t)}{dx} dx - \frac{1}{2} \int_{I_j} A(t) w (w - 2(A(t)x + B(t))) dx. \tag{3.17}$$

Summing over all j, we obtain

$$\begin{aligned}
&\int_I w_{ht} w_h dx + \sum_j \left(-F((w_h)^-_{j+\frac{1}{2}}, x, t) + F((w_h)^+_{j-\frac{1}{2}}, x, t) + \widehat{f}_{j+\frac{1}{2}}(w_h)^-_{j+\frac{1}{2}} - \widehat{f}_{j-\frac{1}{2}}(w_h)^+_{j-\frac{1}{2}} \right) \\
&+ \epsilon \sum_j \left(-\frac{1}{2}(w^2_{hx})^-_{j+\frac{1}{2}} + \frac{1}{2}(w^2_{hx})^+_{j-\frac{1}{2}} \right) + \epsilon \sum_j \left((\widehat{w_{hxx}})_{j+\frac{1}{2}}(w_h)^-_{j+\frac{1}{2}} - (\widehat{w_{hxx}})_{j-\frac{1}{2}}(w_h)^+_{j-\frac{1}{2}} \right) \\
&+ \epsilon \sum_j \left(((w_{hx})^-_{j+\frac{1}{2}} - (\widehat{w_{hx}})_{j+\frac{1}{2}})(w_{hx})^-_{j+\frac{1}{2}} - ((w_{hx})^+_{j-\frac{1}{2}} - (\widehat{w_{hx}})_{j-\frac{1}{2}})(w_{hx})^+_{j-\frac{1}{2}} \right) \\
&+ \epsilon \sum_j \left(((\widehat{w_h})_{j+\frac{1}{2}} - (w_h)^-_{j+\frac{1}{2}})(w_{hxx})^-_{j+\frac{1}{2}} - ((\widehat{w_h})_{j-\frac{1}{2}} - (w_h)^+_{j-\frac{1}{2}})(w_{hxx})^+_{j-\frac{1}{2}} \right) \\
&= \int_{I_j} r w_h dx + \frac{1}{2} \int_{I_j} A(t) w (w - 2(A(t)x + B(t))) dx.
\end{aligned} \tag{3.18}$$

Let $\mathcal{E}(I)$ denotes the interior cell interfaces of interval I. Now we regroup (3.18) with interior and boundary terms denoted by I^I and I^B,

$$\frac{1}{2}\frac{d}{dt}\|w_h(\cdot,t)\|^2 + I^I + I^B \leqslant \frac{1}{2}\|r(\cdot,t)\|^2 + \frac{1}{2}\|w_h(\cdot,t)\|^2 + \frac{1}{2}\int_I A(t) w (w - 2(A(t)x + B(t))) dx, \tag{3.19}$$

where I^I is defined by

$$I^I := \sum_{\mathcal{E}(I)} \left([F(w_h, x, t)] - \widehat{f}[w_h] \right) + \epsilon \sum_{\mathcal{E}(I)} \left(\frac{1}{2}[w^2_{hx}] \right) - \epsilon \sum_{\mathcal{E}(I)} (\widehat{w_{hxx}}[w_h]) - \epsilon \sum_{\mathcal{E}(I)} ([w^2_{hx}] - \widehat{w_{hx}}[w_{hx}]) - \epsilon \sum_{\mathcal{E}(I)} (\widehat{w_h}[w_{hxx}] - [w_h w_{hxx}]),$$

and I^B collects all boundary terms,

$$\begin{aligned}
&I^B : \\
&= \left(-F((w_h)^-_{N+\frac{1}{2}}, x, t) + F((w_h)^+_{\frac{1}{2}}, x, t) + \widehat{f}_{N+\frac{1}{2}}(w_h)^-_{N+\frac{1}{2}} - \widehat{f}_{\frac{1}{2}}(w_h)^+_{\frac{1}{2}} \right) + \epsilon \left(-\frac{1}{2}(w^2_{hx})^-_{N+\frac{1}{2}} + \frac{1}{2}(w^2_{hx})^+_{\frac{1}{2}} \right) \\
&+ \epsilon \left((\widehat{w_{hxx}})_{N+\frac{1}{2}}(w_h)^-_{N+\frac{1}{2}} - (\widehat{w_{hxx}})_{\frac{1}{2}}(w_h)^+_{\frac{1}{2}} \right) + \epsilon \left(((w_{hx})^-_{N+\frac{1}{2}} - (\widehat{w_{hx}})_{N+\frac{1}{2}})(w_{hx})^-_{N+\frac{1}{2}} - ((w_{hx})^+_{\frac{1}{2}} - (\widehat{w_{hx}})_{\frac{1}{2}})(w_{hx})^+_{\frac{1}{2}} \right) \\
&+ \epsilon \left(((\widehat{w_h})_{N+\frac{1}{2}} - (w_h)^-_{N+\frac{1}{2}})(w_{hxx})^-_{N+\frac{1}{2}} - ((\widehat{w_h})_{\frac{1}{2}} - (w_h)^+_{\frac{1}{2}})(w_{hxx})^+_{\frac{1}{2}} \right).
\end{aligned}$$

Using the numerical fluxes $(\widehat{w_{hxx}})_{j+\frac{1}{2}}, (\widehat{w_{hx}})_{j+\frac{1}{2}}, (\widehat{w_h})_{j+\frac{1}{2}}, \widehat{f}$, as described in (3.13) and (3.14), we find that all terms in I^I are canceled, then

$$I^I = 0.$$

We now turn to estimate I^B. Using boundary fluxes defined in (3.13) and (3.14), for the terms related to the right boundary $x_{N+1/2}$, we estimate as follows:

$$\begin{aligned}
-F((w_h)^-_{N+\frac{1}{2}}, x, t) + \widehat{f}_{N+\frac{1}{2}}(w_h)^-_{N+\frac{1}{2}} &= F((w_h)^+_{N+\frac{1}{2}}, x, t) - F((w_h)^-_{N+\frac{1}{2}}, x, t) + \widehat{f}_{N+\frac{1}{2}}(w_h)^-_{N+\frac{1}{2}} - \widehat{f}_{N+\frac{1}{2}}(w_h)^+_{N+\frac{1}{2}} \\
&= \int_{(w_h)^-_{N+\frac{1}{2}}}^{(w_h)^+_{N+\frac{1}{2}}} (f(s, x, t) - \widehat{f}_{N+\frac{1}{2}}) ds = 0,
\end{aligned}$$

$$\begin{aligned}
-\epsilon \frac{1}{2}(w^2_{hx})^-_{N+\frac{1}{2}} + \epsilon((w_{hx})^-_{N+\frac{1}{2}} - (\widehat{w_{hx}})_{N+\frac{1}{2}})(w_{hx})^-_{N+\frac{1}{2}} &= \epsilon \frac{1}{2}(w^2_{hx})^-_{N+\frac{1}{2}} - \epsilon g(t)(w_{hx})^-_{N+\frac{1}{2}} \\
&= \epsilon \frac{1}{2}\left((w_{hx})^-_{N+\frac{1}{2}} - g(t) \right)^2 - \epsilon \frac{1}{2} g(t)^2 \geqslant -\epsilon \frac{1}{2} g(t)^2,
\end{aligned}$$

$$\epsilon(\widehat{w_{hxx}})_{N+\frac{1}{2}}(w_h)^-_{N+\frac{1}{2}} + \epsilon((\widehat{w_h})_{N+\frac{1}{2}} - (w_h)^-_{N+\frac{1}{2}})(w_{hxx})^-_{N+\frac{1}{2}} = 0.$$

Similarly terms involving the left boundary $x_{1/2}$ reduce to

$$F((w_h)^+_{\frac{1}{2}}, x, t) + \widehat{f}_{\frac{1}{2}}(w_h)^+_{\frac{1}{2}} = \int_{(w_h)^-_{\frac{1}{2}}}^{(w_h)^+_{\frac{1}{2}}} (f(s,x,t) - \widehat{f}_{\frac{1}{2}})ds = 0,$$

$$\epsilon\frac{1}{2}(w^2_{hx})^+_{\frac{1}{2}} - \epsilon((w_{hx})^+_{\frac{1}{2}} - (\widehat{w_{hx}})_{\frac{1}{2}})(w_{hx})^+_{\frac{1}{2}} = \epsilon\frac{1}{2}(w^2_{hx})^+_{\frac{1}{2}} \geqslant 0 - \epsilon(\widehat{w_{hxx}})_{\frac{1}{2}}(w_h)^+_{\frac{1}{2}} - \epsilon((\widehat{w_h})_{\frac{1}{2}} - (w_h)^+_{\frac{1}{2}})(w_{hxx})^+_{\frac{1}{2}} = 0.$$

Gathering together the above estimates, we have

$$I^B \geqslant -\frac{\epsilon}{2}g(t)^2.$$

Notice $I^I = 0$ and the Schwatz inequality, inequality (3.19) becomes

$$\frac{1}{2}\frac{d}{dt}\|w_h(\cdot,t)\|^2 \leqslant \left(\frac{1}{2} + |A(t)|\right)\|w_h(\cdot,t)\|^2 + \epsilon\frac{1}{2}g^2(t) + \frac{1}{2}|A(t)|\|A(t)x + B(t)\|^2 + \frac{1}{2}\|r(\cdot,t)\|^2.$$

By the Gronwall inequality, we obtain the desired estimate.

We now establish the stability for the DDG method applied to the original problem. Let $u(x,t)$ denote the solution of the original problem (3.1). Using the transformation (3.9), one can convert the original problem (3.1) to the auxiliary problem (3.10). Applying the L^2 stability estimation stated in Proposition 3.1 we are able to summarize the L^2 stability of DDG method for the IBVP (3.1) as follows:

Theorem 3.2. *The L^2 norm of the numerical solution of (3.1) is bounded by the initial and boundary data*

$$\|u_h(\cdot,t)\| \leqslant K(a_1(t), a_2(t), b(t), \|u_h(0)\|), \quad \forall t \in [0,T].$$

3.3. Time discretization

For the IBVP with general boundary conditions, in addition to the second order Crank-Nicolson time discretization, we also consider the backward Euler scheme for the time discretization.

Let $\{t^n\}, n = 0, 1, \ldots, M$ be a uniform partition of the time interval $[0,T]$. Set $\Delta t = t^{n+1} - t^n$ to denote the time step. The fully-discrete DDG method for the KdV equation is to find $u_h^n \in V_h$ such that

$$\begin{aligned}\int_{I_j}\frac{u_h^{n+1}-u_h^n}{\Delta t}v dx - \int_{I_j} f(u_h^{n+1})v_x dx - \epsilon\int_{I_j} u_{hxx}^{n+1}v_x dx + \widehat{f}(u_h^{n+1})v\Big|_{j-\frac{1}{2}}^{j+\frac{1}{2}} + \epsilon\widehat{u_{hxx}^{n+1}}\,v\Big|_{j-\frac{1}{2}}^{j+\frac{1}{2}} + \epsilon(u_{hx}^{n+1} - \widehat{u_{hx}^{n+1}})v_x\Big|_{j-\frac{1}{2}}^{j+\frac{1}{2}} \\ + \epsilon(\widehat{u_h^{n+1}} - u_h^{n+1})v_{xx}\Big|_{j-\frac{1}{2}}^{j+\frac{1}{2}} = 0, \forall v \in V_h \end{aligned} \tag{3.20}$$

with $u_h^0 = Pu_0$ the piecewise L^2 projection of $u_0(x)$. The backward Euler scheme, though only first order in time, is easy to implement in capturing various wave patterns near boundary.

4. Numerical examples

In this section, we present some numerical examples to demonstrate the accuracy and capacity of the DDG method for the KdV equation. For the IVP with periodic boundary conditions, we illustrate the conservative properties of the schemes; For the IBVP with general boundary conditions, we show the capability of the method in capturing various boundary wave patterns. In the numerical examples, the Gauss–Legendre 16 point quadrature rule is used for numerical integration.

4.1. Initial value problem

Example 4.1. We consider the IVP of the KdV equation

$$\begin{cases} u_t + uu_x + \epsilon u_{xxx} = 0, & x \in (0,1), t > 0, \\ u(x,0) = u_0(x), & x \in (0,1), \end{cases} \tag{4.1}$$

with periodic boundary conditions. The exact solution is the so-called cnoidal-wave solution,

$$u(x,t) = acn^2(4K(m)(x - vt - x_0)),$$

Table 1
Cnoidal-wave problem, $k = 2$, uniform mesh with N cells.

	N	Δt	L^2 error	Order		N	Δt	L^2 error	Order
$\theta = 0$	20	1.0e−02	1.27882e−00	–	$\theta = 1$	20	1.0e−02	1.27515e−00	–
	40	2.5e−03	1.78694e−01	2.8393		40	2.5e−03	1.78692e−01	2.8351
	80	6.25e−04	1.20167e−02	3.8944		80	6.25e−04	1.20205e−02	3.8939
	160	1.5625e−04	7.57514e−04	3.9533		160	1.5625e−04	7.5839e−04	3.9864
	320	3.90625e−05	4.79678e−05	4.0155		320	3.90625e−05	4.79678e−05	3.9828
$\theta = \frac{1}{4}$	20	1.0e−02	8.48863e−01	–	$\theta = \frac{1}{5}$	20	1.0e−02	1.23842e−00	–
	40	2.5e−03	1.3451e−01	2.6578		40	2.5e−03	1.41597e−01	3.1286
	80	6.25e−04	8.15008e−03	4.0448		80	6.25e−04	8.73187e−03	4.0194
	160	1.5625e−04	4.98486e−04	4.0312		160	1.5625e−04	5.36009e−04	4.0206
	320	3.90625e−05	3.11224e−05	4.0015		320	3.90625e−05	3.34842e−05	4.0007
$\theta = \frac{1}{2}$	20	1.0e−02	5.80566e−01	–	$\theta = \frac{2}{5}$	20	1.0e−02	9.58565e−01	–
	40	2.5e−03	1.17805e−01	2.3011		40	2.5e−03	1.20566e−01	2.9911
	80	6.25e−04	6.80724e−03	4.0921		80	6.25e−04	7.02521e−02	4.1011
	160	1.5625e−04	4.10563e−04	4.0724		160	1.5625e−04	4.2499e−04	4.0470
	320	3.90625e−05	2.59839e−05	3.9819		320	3.90625e−05	2.68425e−05	3.9848
$\theta = \frac{3}{4}$	20	1.0e−02	1.06497e−00	–	$\theta = \frac{4}{5}$	20	1.0e−02	1.21731e−00	–
	40	2.5e−03	1.34509e−01	2.9850		40	2.5e−03	1.41596e−01	3.1038
	80	6.25e−04	8.15007e−03	4.0448		80	6.25e−04	8.73187e−03	4.0193
	160	1.5625e−04	4.98485e−04	4.0312		160	1.5625e−04	5.36009e−04	4.0260
	320	3.90625e−05	3.11223e−05	4.0015		320	3.90625e−05	3.34842e−05	4.0007

where $cn(z) = cn(z|m)$ is the Jacobi elliptic function with modulus $m = 0.9$ and the parameters have the values $a = 192m\epsilon K^2(m)$, $\nu = 64\epsilon(2m-1)K^2(m)$, and $x_0 = 1/2$. The function $K = K(m)$ is the complete elliptic integral of the first kind. This example is derived from [2].

In this example, we take $\epsilon = 1/24^2$, and the computational domain is divided into N cells. We test the $P^k, k = 2, 3, 4$ polynomial approximation on uniform meshes. For the time discretization, we employ the second order Crank–Nicholson scheme for $k = 2, 3$, and take a two-stage implicit Runge–Kutta method of Gauss–Legendre type time discretization [3] for $k = 4$. This method is fourth order in time. We set the time-step Δt by the relation $\Delta t = Ch^2$ with the spatial-step size $h = 1/N$. This choice guarantees that the error will be dominated by the spatial discretization. We first test the order of accuracy calculated by

$$order = \frac{\log(e(N))/\log(e(2N))}{\log(2)},$$

where $e(N)$ is the L^2-error $\|u(\cdot,t) - u_h(\cdot,t)\|$ at $t = 10$ made using N cells in the spatial approximation. Table 1 reports the numerical errors and the orders of accuracy for $k = 2$ with different $\theta \in [0,1]$ at $t = 10$; Different choices of $\theta \in [0,1]$ are shown to yield the same order of accuracy. Tables 2,3 show the numerical errors and the orders of accuracy for $k = 3, 4$ with $\theta = 0, 1$. We observe that the scheme is only third order for $k = 3$, but fifth order for $k = 4$ as expected. However, in the case of $k = 2$ we observe a special fourth-order accuracy, though the reasoning behind this superconvergence remains to be disclosed.

We now verify the conservative property of the DDG method, and compare it with a non-conservative DDG method. In what follows, DDG-C is used to denote our DDG method with conservative numerical fluxes

$$\left(\widehat{f}(u_h), \widehat{u_{hxx}}, \widehat{u_{hx}}, \widehat{u_h}\right) = \left(\fint_{u_h^-}^{u_h^+} f(u)du, u_{hxx}^+, \{u_{hx}\}, u_h^-\right);$$

The DDG-NC method denotes the DDG method with non-conservative numerical fluxes

$$\left(\widehat{f}(u_h), \widehat{u_{hxx}}, \widehat{u_{hx}}, \widehat{u_h}\right) = \left(\frac{1}{2}(f(u_h^-) + f(u_h^+) - \sigma(u_h^+ - u_h^-)), u_{hxx}^+, u_{hx}^+, u_h^-\right),$$

where $\sigma = \max|f'(u_h)|$. Using the cnoidal-wave test problem with $k = 2$ and $\Delta t = 0.000625$, we plot in Fig. 1 the L^2 energy from $t = 0$ to $t = 200$ of the two proposed methods, DDG-C and DDG-NC respectively. We can see that the energy of the DDG-NC method is dissipative, but the DDG-C method have the conservative property

$$\|u_h^n\| = \|u_h^0\|, \quad n = 1, 2, \ldots.$$

Fig. 2 plots the numerical solutions of the DDG-C method and DDG-NC method at $t = 10$ and $t = 200$. The exact solution is provided as a reference in the plot. The DDG-NC method has a large phase error, while the DDG-C method gives quite a good approximation to the exact solution. Besides the larger phase error, the amplitude of the wave produced by the DDG-NC method decays as time increases.

Table 2
Cnoidal-wave problem, $k = 3$, uniform mesh with N cells.

	N	Δt	L^2 error	Order		N	Δt	L^2 error	Order
$\theta = 0$	20	1.0e−02	1.55079e−01	–	$\theta = 1$	20	1.0e−02	1.58092e−01	–
	40	2.5e−03	1.21104e−02	3.6787		40	2.5e−03	1.21529e−02	3.7014
	80	6.25e−04	1.20400e−03	3.3303		80	6.25e−04	1.20458e−03	3.3347
	160	1.5625e−04	1.41081e−04	3.0932		160	1.5625e−04	1.40925e−04	3.0955

Table 3
Cnoidal-wave problem, $k = 4$, uniform mesh with N cells.

	N	Δt	L^2 error	Order		N	Δt	L^2 error	Order
$\theta = 0$	20	1.0e−02	8.41007e−03	–	$\theta = 1$	20	1.0e−02	8.31945e−03	–
	40	2.5e−03	4.33721e−06	10.921		40	2.5e−03	4.17746e−06	10.960
	80	6.25e−04	7.61342e−08	5.832		80	6.25e−04	7.61282e−08	5.7781
	160	1.5625e−04	2.65901e−09	4.840		160	1.5625e−04	2.62996e−09	4.8553

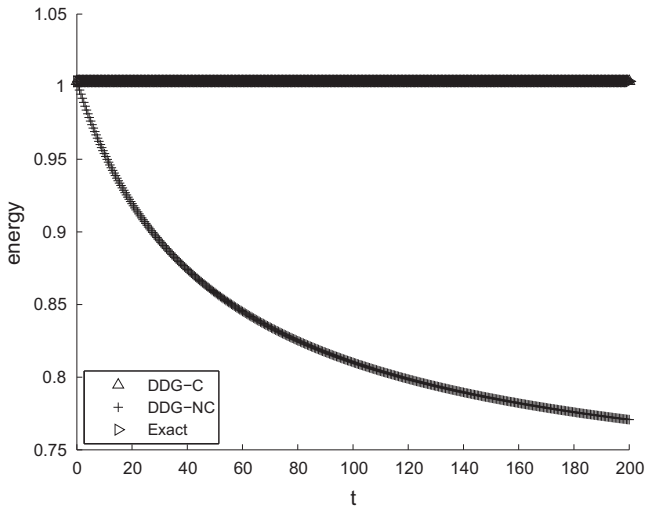

Fig. 1. Example 4.1, time history of the L^2 energy plots using the DDG-C and DDG-NC methods with $k = 2$ and 80 cells.

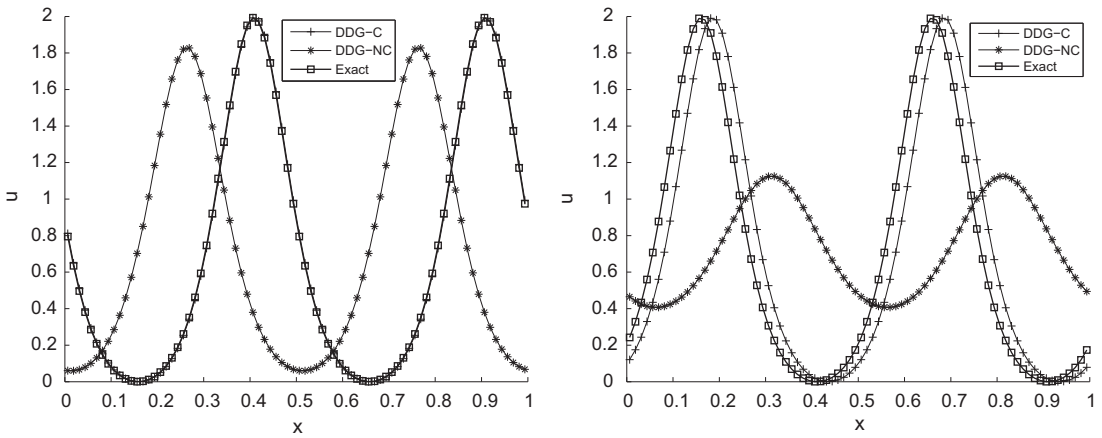

Fig. 2. Example 4.1, solution plots using the DDG-C and DDG-NC methods with $k = 2$ and 80 cells; comparisons at different times. Left: time $t = 10$; Right: time $t = 200$.

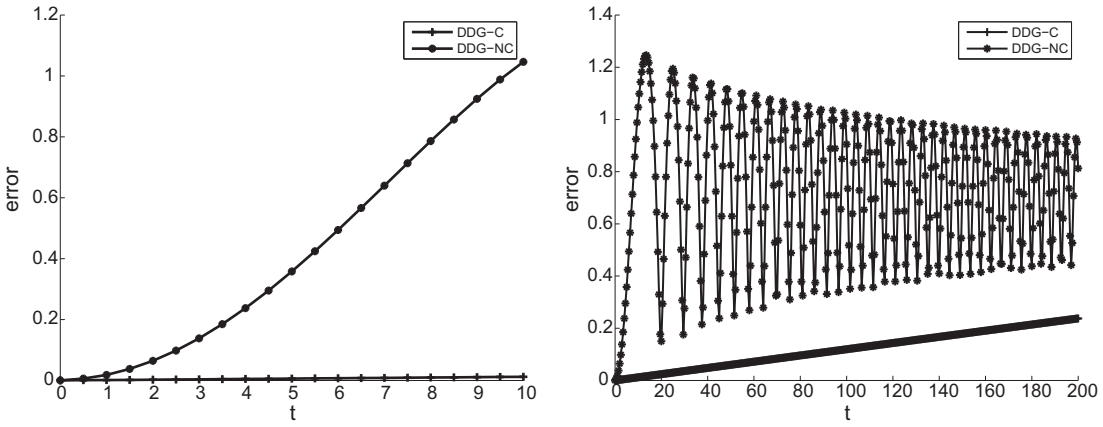

Fig. 3. Example 4.1, time history of the L^2 error $\|u(\cdot,t)-u_h(\cdot,t)\|$ plots using the DDG-C and DDG-NC methods with $k=2$ and 80 cells. Left: L^2 error for $t\in[0,10]$; Right: L^2 error for $t\in[0,200]$.

We also present the time evolution of the L^2-error $\|u(\cdot,t)-u_h(\cdot,t)\|$ up to time $t=10$ and $t=200$ in Fig. 3. It shows that the L^2-error of the conservative method has much smaller error. Indeed, at time $t=10$, the error of the DDG-NC method is about 87 times larger than that of the DDG-C method. The L^2-error of the DDG-C method increases linearly with time.

Example 4.2. Consider again the KdV Eq. (4.1) with $\epsilon=1$, and $u(x,0)$ as the initial data, the exact solution is of the two soliton waves

$$u(x,t)=12\frac{k_1^2e^{\theta_1}+k_2^2e^{\theta_2}+2(k_2-k_1)^2e^{\theta_1+\theta_2}+a^2(k_2^2e^{\theta_1}+k_1^2e^{\theta_2})e^{\theta_1+\theta_2}}{(1+e^{\theta_1}+e^{\theta_2}+a^2e^{\theta_1+\theta_2})^2}, \tag{4.2}$$

where

$$k_1=0.4,\quad k_2=0.6,\quad a^2=\left(\frac{k_1-k_2}{k_1+k_2}\right)^2=\frac{1}{25},\quad \theta_1=k_1x-k_1^3t+x_1,\quad \theta_2=k_2x-k_2^3t+x_2,\quad x_1=4,\quad x_2=15.$$

This example is derived from [35]. The solution region is taken to be $[-40,40]$ with periodic boundary conditions. Initially we have two solitons, the left tall one and the right short one. Both solitons travel from left to right, and speed of the tall one is bigger than the speed of the short one. We perform computation for $k=2$ and $\Delta t=0.1$. The grid is taken to be of 400 cells and the computation is implemented up to $t=120$.

The numerical solution at four different times are plotted in Fig. 4. It shows that the numerical solution agrees quite well with the exact one. The interaction process can be visualized from a series of snapshots: $t=0$ (two peaks), $t=40$ (the tall one catches up the short one), $t=80$ (overlap), $t=120$ (the tall one over takes the short one).

Example 4.3. We consider the Zabusky-Kruskal's problem, setting the dispersion coefficient $\epsilon=0.022^2$ and

$$u(x,0)=\cos(\pi x), \tag{4.3}$$

with periodic boundary conditions. The solution starts with a cosine wave and latter on develops a train of 8 solitons which travel at different speeds and interact with each other, see [42] for detailed description of the solution. There are several critical moments in the development of the solution: (1) $t=t_B=\frac{1}{\pi}$ when the solution is about to breakdown, (2) $t=3.6t_B$ when a train of 8 solitons have been developed.

We perform computation on 400 cells with $k=2$ and $\Delta t=\frac{0.005}{\pi}$. We carry out the computation to the time $t=t_B$ and $t=3.6t_B$, the initial values and the numerical solution at the two times are plotted in Fig. 5. It shows that all of them agree quite well with the numerical result obtained by Zabusky and Kruskal in 1965, see [42].

4.2. IBVP with general boundary conditions

Numerical examples in this subsection are taken from [24], for which the KdV eqaution is posed on a finite domain $x\in[-M,0]$, with boundary conditions

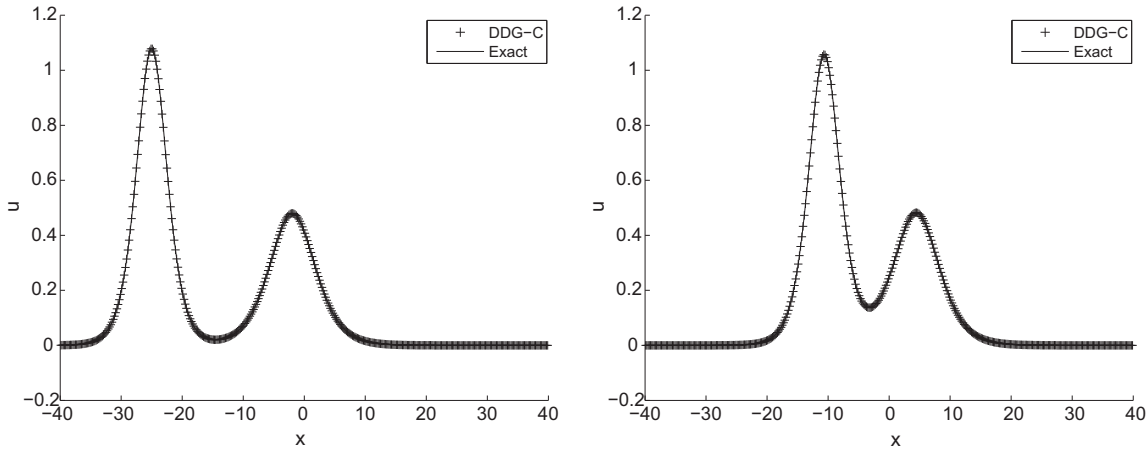

(a) Numerical solution at $t = 0$. (b)Numerical solution at $t = 40$.

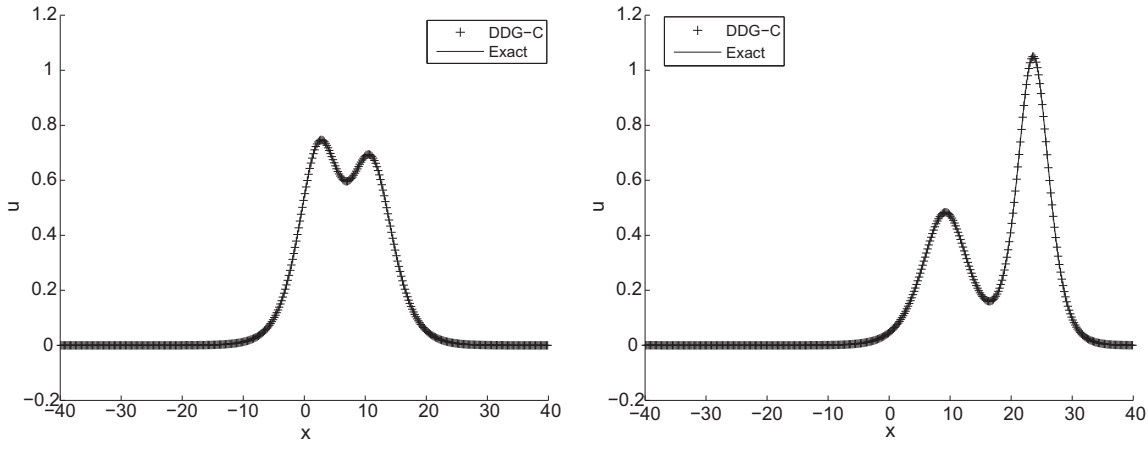

(c) Numerical solution at $t = 80$. (d)Numerical solution at $t = 120$.

Fig. 4. Example 4.2, solution plots using the DDG method with $\theta = 1.0, k = 2$ and 400 cells at different times.

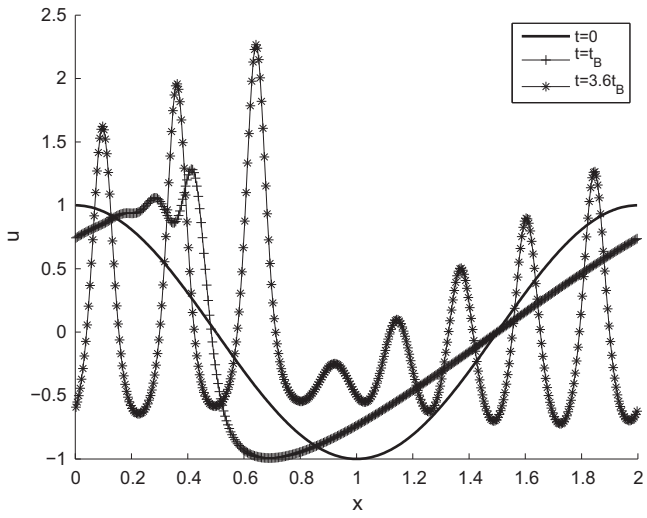

Fig. 5. Example 4.3, numerical solution plots at $t = 0, t_B$ and $3.6t_B, \theta = 1.0, k = 2, 400$ cells.

Table 4
Computational domain Ω is $[-10,0], u(x,0) = 2sech^2(x+4), L^2$ errors, DDG method with $k = 2,3$ at $t = 0.75$, uniform mesh with N cells.

θ	k	Δt	N = 20	N = 40		N = 80		N = 160	
			Error	Error	Order	Error	Order	Error	Order
0.0	2	h^3	0.37618	0.0438029	3.10	0.00535372	3.03	0.000667256	3.00
	3	h^4	0.187945	0.0106963	4.14	0.000670609	4.00	4.26636e−05	3.97
1.0	2	h^3	0.369723	0.0438627	3.07	0.00535876	3.03	0.000667613	3.00
	3	h^4	0.188361	0.0107041	4.14	0.000670818	4.00	4.26729e−05	3.97

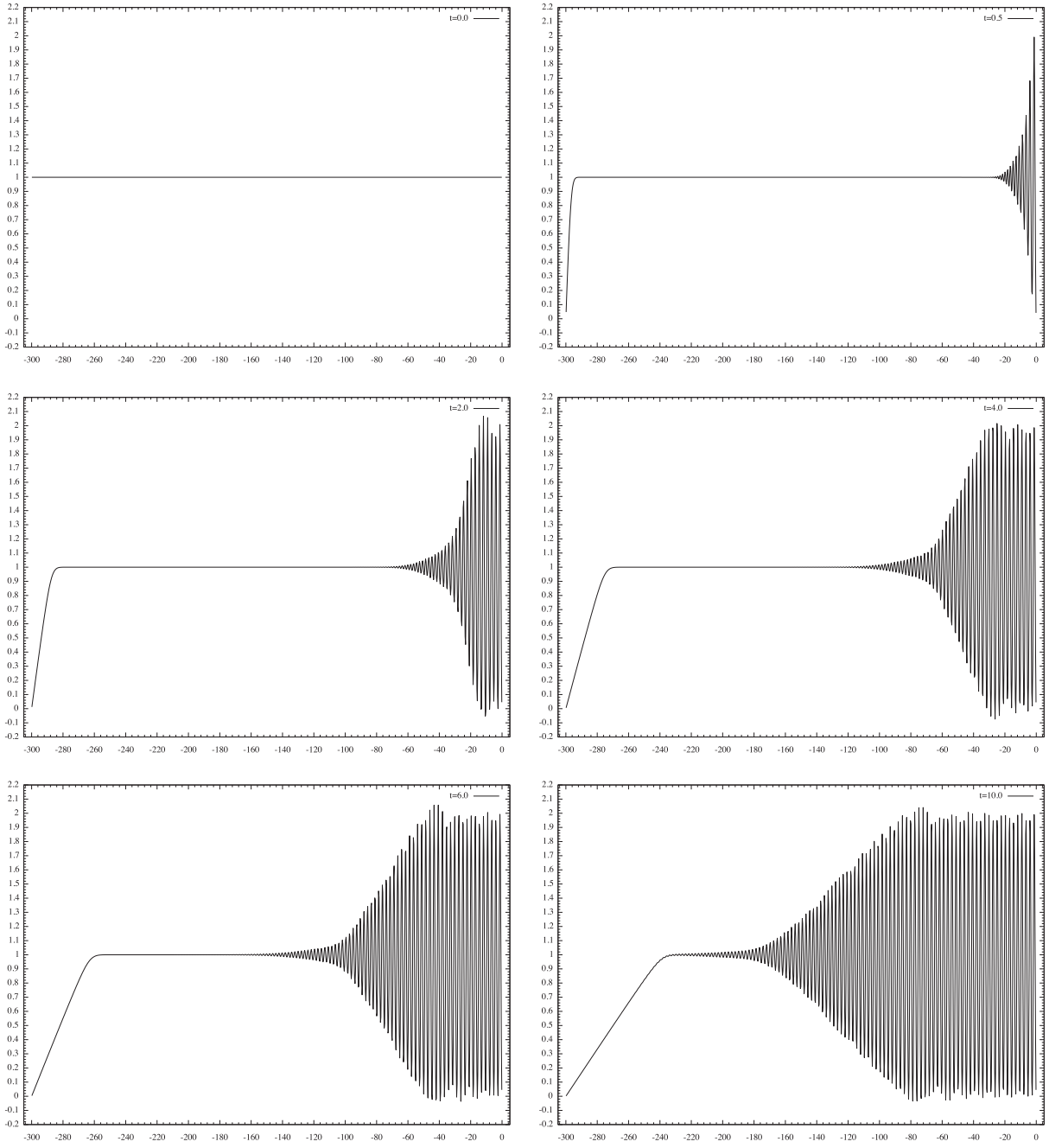

Fig. 6. Example 4.5, $u_0(x) = 1.0, u(-300,t) = 0.0, u(0,t) = 0.0, u_x(0,t) = 0.0$ with $\theta = 1.0, P^3$ polynomials and 1000 cells at $t = 0, 0.5, 2.0, 4.0, 6.0$ and 10.0.

Table 5
The L^2 norm at different time for Example 4.5 with P^3 polynomials and $\theta = 1.0$.

N = 1000	T = 0	T = 0.5	T = 1	T = 2	T = 4	T = 6	T = 8	T = 10
$\|u_h\|/\|u\|$	1.0000	0.9981	0.9980	0.9978	0.9975	0.9972	0.9968	0.9963

$$\begin{cases} u_t + 6uu_x + u_{xxx} = 0, & x \in [-M, 0], \\ u(x,0) = u_0(x), & x \in [-M, 0], \\ u(-M,t) = 0, u(0,t) = a(t), & t > 0, \\ u_x(0,t) = b(t), & t > 0. \end{cases} \tag{4.4}$$

Example 4.4. Accuracy test.

We compute the classical soliton solution of the KdV equation in $[-10, 0]$. The initial condition is given by

$$u(x,0) = 2sech^2(x+4)$$

and the exact solution is

$$u(x,t) = 2sech^2(x+4-ct), \quad c = 4.$$

For boundary conditions $u(-10,t), u(0,t)$ and $u_x(0,t)$, we simply use the values extracted from the exact solution. The second order Crank–Nicolson time discretization is employed in this example. The L^2 errors are reported in Table 4 for $t = 0.75$. It shows that the DDG method with P^k element gives $(k+1)$th order of accuracy.

Next we illustrate the capacity of our method in capturing the boundary wave patterns through a series of examples of the form (4.4). When M is large enough, the results may be regarded as valid for the half-space problem

$$\begin{cases} u_t + 6uu_x + u_{xxx} = 0, & x \in (-\infty, 0], \\ u(x,0) = u_0(x), & x \in (-\infty, 0], \\ u(0,t) = a(t), & t > 0, \\ u_x(0,t) = b(t), & t > 0. \end{cases} \tag{4.5}$$

A particular solution of the KdV equation is the conoidal wave expressed in terms of the mean height $\bar{u}$, the amplitude A, phase shift ϕ, wave number and dispersion relation. A special case of the conoidal wave is the soliton solution

$$u = \bar{u} + 2Asech^2\sqrt{A}[x - (6\bar{u} + 4A)t + \phi]. \tag{4.6}$$

We numerically simulate the five typical wave patterns as studied in [29] and tested in [24] by the LDG method, subject to constant initial and boundary data with

$$a(t) = a \in \mathbb{R}, \quad b(t) = 0, \quad u_0(x) = u_0 \in \mathbb{R}.$$

We observed the similar phenomenon as those in [24], except for one boundary wave pattern in Fig. 8 of [24]. The test by the DDG method clearly produces a more oscillatory wave pattern than that in [24] Fig. 8. We choose to only present this example.

Example 4.5. Boundary wave pattern.

The initial and boundary data are in the form of

$$\begin{cases} u_0(x) = 1.0, & x \in [-300, 0], \\ a(t) = 0.0, & t > 0, \\ b(t) = 0.0, & t > 0. \end{cases}$$

The right boundary condition and the initial data satisfies $a \geqslant u_0 \geqslant a/4$, in this case a steady conoidal wave formed near the boundary, matched by a partial undular bore $(0 \leqslant m \leqslant m_0 < 1)$ in order to bring the mean level up to u_0 and so to satisfy the initial condition

$$u = \begin{cases} \text{steady conoidal wave}, & r_f t \leqslant x \leqslant 0, \\ \text{partial undular bore}, & 6(u_0 - 2A_0/m_0)t \leqslant x \leqslant r_f t, \\ u_0, & x < 6(u_0 - 2A_0/m_0)t, \end{cases}$$

where $m_0 = \frac{2(a-u_0)}{a+2u_0}, A_0 = a - u_0$ and $r_f = 6u_0 + 2A_0 - 4A_0 m_0^{-1} - \frac{4A_0(1-m_0)}{P(m_0)-(1-m_0)}$, see [29].

Numerical results are shown in Fig. 6. It shows that a conoidal wave is formed near the right boundary matched to a partial undular bore to further connect to the left bigger initial data. Though the solution has strong oscillatory wave patterns, the L^2 energy shown in Table 5 is well conserved by the proposed DDG method, in sharp contrast to the energy dissipation induced by the LDG method [24] Table 4.

Acknowledgments

Yi's research was supported by NSFC Project (11201397), Hunan Education Department Project (12B127), and Hunan Provincial NSF Project (12JJ4004). Huang's research was supported in part by the NSFC Key Project (11031006), Hunan Provincial NSF Project (10JJ7001), and Hunan Education Department Key Project (10A117). Liu's research was partially supported by the National Science Foundation under Grant DMS09-07963.

References

[1] D.N. Arnold, R. Winther, A superconvergent finite element method for the Korteweg–de Vries equation, Math. Comp. 38 (1982) 23–36.
[2] J. Bona, H. Chen, O. Karakashian, and Y. Xing. Conservative, discontinuous-Galerkin methods for the generalized Korteweg–de Vries equation, Preprint.
[3] J.C. Butcher, Implicit Runge–Kutta processes, Math. Comp. 18 (1964) 50–64.
[4] C. Carstensen, R.H.W. Hoppe, N. Sharma, T. Warburton, Adaptive hybridized interior penalty discontinuous Galerkin methods for H(curl)-elliptic problems, Numer. Math. Theory Methods Appl. 4 (2011) 13–37.
[5] Y. Cheng, C.W. Shu, A discontinuous Galerkin finite element method for time dependent partial differential equations with higher order derivatives, Math. Comp. 77 (2008) 699–730.
[6] Y. Cui, D. Mao, Numerical method satisfying the first two conservation laws for the Korteweg–de Vries equation, J. Comput. Phys. 227 (2007) 376–399.
[7] B. Cockburn, S.-Y. Lin, C.-W. Shu, TVB Runge–Kutta local projection discontinuous Galerkin finite element method for conservation laws III: one dimensional systems, J. Comput. Phys. 84 (1989) 90–113.
[8] B. Cockburn, C.-W. Shu, TVB Runge–Kutta local projection discontinuous Galerkin finite element method for conservation laws II: general framework, Math. Comput. 52 (1989) 411–435.
[9] B. Cockburn, S. Hou, C.-W. Shu, The Runge–Kutta local projection discontinuous Galerkin finite element method for conservation laws IV: the multidimensional case, Math. Comput. 54 (1990) 545–581.
[10] B. Cockburn, C.-W. Shu, The Runge–Kutta discontinuous Galerkin method for conservation laws V: multidimensional systems, J. Comput. Phys. 141 (1998) 199–224.
[11] M. Dahlby, B. Owren, A general framework for deriving integral-preserving numerical methods for PDEs, SIAM J. Sci. Comput. 33 (2011) 2318–2340.
[12] B. Fornberg, G.B. Whitham, A numerical and theoretical study of certain nonlinear wave phenomena, Philosophical Transactions of the Royal Society of London. Series A, Mathematical and Physical Sciences 289 (1978) 373–404.
[13] D. Furihata, Finite difference schemes for $\frac{\partial u}{\partial t} = \left(\frac{\partial}{\partial x}\right)^{\alpha} \frac{\delta g}{\delta u}$ that inherit energy conservation or dissipation property, J. Comput. Phys. 156 (1999) 181–205.
[14] K. Goda, Numerical studies on recurrence of the Korteweg–de Vries equation, J. Phys. Soc. Japan 42 (1977) 1040–1046.
[15] I.S. Greig, J.L. Morris, A hopscotch method for the Korteweg–de Vries equation, J. Comput. Phys. 20 (1976) 64–80.
[16] B. Guo, J. Shen, On spectral approximations using modified Legendre rational functions: application to the Korteweg–de Vries equation on the half line, Indiana Univ. Math. J. 50 (2001) 181–204.
[17] H. Holden, K.H. Karlsen, N.H. Risebro, Operator splitting methods for generalized Korteweg–de Vries equations, J. Comput. Phys. 153 (1999) 203–222.
[18] Helge Holden, Kenneth H. Karlsen, Nils Henrik Risebro, Terence Tao, Operator splitting for the KdV equation, Math. Comp. 80 (274) (2011) 821–846.
[19] J. Hu, Y. Huang, A priori and a posteriori error analysis of the discontinuous Galerkin methods for Reissner–Mindlin plates, Adv. Appl. Math. Mech. 3 (2011) 649–662.
[20] W. Huang, D.M. Sloan, The pseudospectral method for third-order differential equations, SIAM J. Numer. Anal. 29 (1992) 1626–1647.
[21] D.J. Korteweg, G. de Vries, On the change of form of long waves advancing in a rectangular canal, and on a new type of long stationary waves, Philos. Mag. 39 (1895) 422–443.
[22] P. Lax, Integrals of nonlinear equations of evolution and solitary waves, Commun. Pure Appl. Math. 21 (1968) 467–490.
[23] J. Li, M.R. Visbal, High-order compact schemes for nonlinear dispersive waves, J. Sci. Comput. 26 (2006) 1–23.
[24] H. Liu, J. Yan, A local discontinuous Galerkin method for the Korteweg–de Vries equation with boundary effect, J. Comput. Phys. 215 (2006) 197–218.
[25] H. Liu, J. Yan, The direct discontinuous Galerkin (DDG) method for diffusion problems, SIAM J. Numer. Anal. 47 (2009) 675–698.
[26] H. Liu, J. Yan, The direct discontinuous Galerkin (DDG) method for diffusion with interface corrections, Commun. Comput. Phys. 8 (2010) 541–564.
[27] H. Ma, W. Sun, A Legendre–Petrov–Galerkin and Chebyshev collocation method for third-order differential equations, SIAM J. Numer. Anal. 38 (2001) 1425–1438.
[28] H. Ma, W. Sun, Optimal error estimates of the Legendre–Petrov–Galerkin method for the Korteweg–de Vries equation, SIAM J. Numer. Anal. 39 (2002) 1380–1394.
[29] T.R. Marchant, N.F. Smyth, The initial boundary problem for the Korteweg–de Vries equation on the negative quarter-plane, Proceedings of the Royal Society of London Series A: Mathematical, Physical and Engineering Sciences 458 (2002) 857–871.
[30] R.M. Miura, C.S. Gardner, M.D. Kruskal, Korteweg–de Vries equation and generalizations ii existence of conservation laws and constants of motion, J. Math. Phys. 9 (1968) 1204–1209.
[31] J.M. Sanz-Serna, I. Christie, Petrov–Galerkin methods for nonlinear dispersive wave, J. Comput. Phys. 39 (1981) 94–102.
[32] J. Shen, A new dual-Petrov–Galerkin method for third and higher odd-order differential equations: application to the KdV equation, SIAM J. Numer. Anal. 41 (2004) 1595–1619.
[33] W. Reed, T. Hill, Triangular mesh methods for the neutron transport equation, LA-UR-73-479, Los Alamos Scientific Laboratory, 1973.
[34] R. Winther, A conservative finite element method for the Korteweg–de Vries equation, Math. Comp. 34 (1980) 23–43.
[35] X.L. Xie, Large time-stepping methods for higher order time-dependent evolution equations, Ph.D. thesis, Iowa State University, Ames, IA, 2008.
[36] Y. Xu, C.W. Shu, Local discontinuous Galerkin methods for two classes of two-dimensional nonlinear wave equations, Physica D: Nonlinear phenom. 208 (2005) 21–58.
[37] Y. Xu, C.W. Shu, Error estimates of the semi-discrete local discontinuous Galerkin method for nonlinear convection-diffusion and KdV equations, Comput. Methods Appl. Mech. Eng. 196 (2007) 3805–3822.
[38] Y. Xu, C.W. Shu, Local discontinuous Galerkin methods for high-order time-dependent partial differential equations, Commun. Comput. Phys. 7 (2010) 1–46.
[39] Y. Xu, C.W. Shu, Local discontinuous Galerkin methods for the Degasperis–Procesi equation, Commun. Comput. Phys. 10 (2011) 474–508.
[40] J. Yan, C.W. Shu, A local discontinuous Galerkin method for KdV type equations, SIAM J. Numer. Anal. 40 (2003) 769–791.
[41] T. Yu, X. Yue, Exponentially fitted local discontinuous Galerkin method for convection-diffusion problems, J. Comp. Math. 30 (2012) 298–310.
[42] N.J. Zabusky, M.D. Kruskal, Interaction of solitons in a collisionless plasma and the recurrence of initial states, Phys. Rev. Lett. 15 (1965) 240–243.